


First-Principles Study of All Thermoelectric Properties of Si-Ge Alloys Showing Large Phonon Drag from 150 to 1100 K

Qian Xu,^{*} Jiawei Zhou, Te-Huan Liu, and Gang Chen[†]

Department of Mechanical Engineering, Massachusetts Institute of Technology, Cambridge, Massachusetts 02139, USA

 (Received 24 August 2021; revised 14 November 2021; accepted 17 November 2021; published 22 December 2021)

Phonon drag due to momentum exchange between electrons and phonons can lead to a substantially increased Seebeck coefficient desirable for thermoelectric energy conversion. However, this effect is only usually observable at low temperatures when the phonon mean free path is long, and it is thought to become negligible above room temperature or in heavily doped materials due to strong phonon scattering. Here, we present first-principles calculations of all thermoelectric transport properties of silicon-germanium alloys from 150 to 1100 K. Results show that phonon drag is dominant at low temperatures. At 1100 K, phonon drag still contributes to 10%–20% of the thermoelectric figure of merit, zT , and its relative contribution increases with higher carrier concentration. The favorable comparison between our calculations and reported experiments brings us closer to predicting the thermoelectric transport properties of alloys using first-principles simulations. The surprising insights in phonon drag could stimulate the search for better thermoelectric materials.

DOI: [10.1103/PhysRevApplied.16.064052](https://doi.org/10.1103/PhysRevApplied.16.064052)

I. INTRODUCTION

Phonon drag due to momentum exchange between traveling phonons driven by a temperature gradient and charge carriers significantly enhances the Seebeck coefficient at low temperatures [1–8]. It is commonly understood that phonon drag is only important at low temperatures ($T \leq 100$ K) and in high-purity materials where phonons have long mean free paths [2]. However, at low temperatures, the lattice thermal conductivity is also large, leading to low thermoelectric-energy-conversion (cooling or power generation) efficiency governed by the dimensionless figure of merit, zT ($zT = S^2 \sigma T / \kappa$, where S , T , σ , and κ are the Seebeck coefficient, the absolute temperature, the electrical conductivity, and the thermal conductivity, respectively). Slack and Hussain [9] pointed out that, in alloy-based thermoelectric materials, like Si-Ge, used to provide power for most deep-space exploration missions [10], the phonon mean free paths are so short that phonon drag would disappear in mixed crystals. However, these assumptions about phonon drag are hard to examine experimentally: it is difficult to determine phonon drag directly from conventional experiments because the measured Seebeck coefficient is the sum of the diffusive and phonon-drag contributions, both of which vary with temperature and doping level. In this work, we use density-functional

theory (DFT) to simulate all thermoelectric transport properties of Si-Ge alloys, including phonon drag, and achieve reasonable agreement with experiments. Strikingly, we find that phonon drag can contribute 10%–20% of zT even up to 1100 K. As a 10%–20% increase in zT is often considered significant in thermoelectric materials, insights into phonon drag's contribution to zT at a comparable level but such high temperatures are of both fundamental and applied importance.

Recent experiments through comparative measurements between bulk and nanostructured materials have shown that phonon drag is still significant in bulk silicon [11], Si nanowires [12], and (Al, Ga)N/GaN two-dimensional electron gas [13] at room temperature. Although these experimental results are inspiring, they require delicate fabrication and measurement techniques, which may not apply to bulk thermoelectric materials in use. Early theoretical works [2,14–16] attempted to quantitatively determine the phonon-drag contribution by solving the coupled electron-phonon Boltzmann transport equations (BTEs) using a variational approach [14], and reasonable agreements with experiments were achieved [17,18]. However, these calculations adopted simplified scattering models with many adjustable parameters, and the quality of the results was much affected by the trial functions. All these impair their predictive power. Mahan *et al.* studied phonon drag in silicon using deformation potentials [19]. Similarly, Protik and Broido solved the coupled BTEs to calculate the transport coefficients of n -doped GaAs using DFT calculations of anharmonic phonon-phonon interactions

^{*}ritaqxu@mit.edu

[†]gchen2@mit.edu

and deformation-potential theory for electron-phonon interactions [20]. Zhou *et al.*, Fiorentini and Bonini further enhanced the predictive power by obtaining the electron-phonon scattering rates from first-principles calculations for silicon [21,22]. Works by Mahan *et al.*, Protik and Broido, and Zhou *et al.* are able to produce results consistent with previous experiments [3,11,23] up to room temperature. The importance of phonon drag at higher temperatures and in alloys typically employed in thermoelectric materials remains unknown.

On the other hand, Klemens [24] pointed out that, in semiconductors, only phonons with a frequency below a critical value, ω_c ($\omega_c \propto T^{1/2}$), would interact with electrons. Zhou *et al.* [21] further show that the major phonons contributing to phonon drag are those with a longer mean free path and lower frequency than those carrying heat. These motivate us to study phonon drag in alloys. It could be possible that the point defects in alloys tend to scatter phonons of short wavelength and high frequency, reducing the lattice thermal conductivity while retaining phonons of long wavelength and consequently long mean free path; thus, phonon drag can still make considerable contributions.

We choose silicon-germanium (Si-Ge) alloys not only because they are one of the best and most-studied high-temperature thermoelectric materials [9,10,25–30], but also phonon drag was reported in germanium [1] and bulk silicon possesses large phonon drag even, at room temperature [19,21]. No previous work has computed all zT parameters in alloys from first principles, despite most high-performance thermoelectric materials employing alloying to reduce thermal conductivity. There are a few DFT-based zT predictions for some nonalloy layered materials [31–33] and three-dimensional (3D) compounds [34–37], most of which use simplified electron-scattering models (e.g., constant relaxation time, energy-dependent relaxation time, deformation-potential theory). In this work, we present DFT simulations of all thermoelectric transport properties of Si-Ge alloys over the complete range of compositions at different concentrations (10^{15} – 10^{20} cm⁻³) from 150 to 1100 K. In particular, we include the phonon-drag contribution in our Seebeck calculations and take alloy scatterings of both phonons and electrons into account. Such detailed simulations not only demonstrate the importance of the phonon-drag effect in practical thermoelectric materials up to 1100 K, but also explain the mechanisms of this persistence and other important aspects of thermoelectric transport in alloys, such as the interplay between band convergence and scattering [38,39]. Our results show that, contrary to what Slack and Hussain assumed above [9], even at 1100 K and at the carrier concentration of 10^{20} cm⁻³, phonon drag is not negligible in Si-Ge alloys: it still contributes to 10%–20% of zT , and its relative contribution increases with carrier concentration in the range of interest. Via spectral analysis of phonon modes, we

attribute this nonintuitive phenomenon to the competition of several phonon-scattering mechanisms. Favorable agreement with reported experimental data proves that our first-principles calculations can provide guidelines for the design of better thermoelectric materials.

II. RESULTS AND DISCUSSION

A. Verification of calculation methodology using silicon as an example

We first verify our method by calculating phonon drag in Si [see Fig. 1(a)]. Good agreement with experimental data [3] at 300 K is achieved across the range of carrier concentrations of interest. We also extend the calculations and plot the results at 150 and 1100 K for comparison. The phonon-drag magnitude is proportional to the momentum transferred from phonons to charge carriers and phonon mean free paths [see Eq. (1) within Supplemental Material Note S1 [41]]. At 150 K, phonon drag is dominant in Si because weak intrinsic phonon scattering results in long phonon mean free paths. Although phonon drag weakens with increasing temperature, it is still comparable to the diffusive part of the Seebeck coefficient, and it constitutes 35%–47% of the total Seebeck coefficient at room temperature in Fig. 1(a). In the lightly doped samples ($n \leq 10^{17}$ cm⁻³), phonon drag is insensitive to the change in carrier concentration because the electron-phonon interaction is so weak that the phonon mean free path is barely affected by it. At higher carrier concentrations, phonon drag starts to drop with increasing carrier concentration, as the phonon mean free path decreases with stronger phonon scattering by electrons [64]. The diffusive Seebeck coefficient represents the average energy that electron transport relative to the Fermi level. At a given temperature, the Fermi level is closer to the band center at lower doping concentrations, which results in the downward trend in the diffusive Seebeck coefficient with increasing carrier concentration. The bipolar contribution to the diffusive Seebeck coefficient is considered at all temperatures, while it is only noticeable at 1100 K when the thermally excited minority charge carriers and majority charge carriers are comparable ($n = 10^{18}$ and 10^{19} cm⁻³ in Fig. 1). Surprisingly, we find, even at 1100 K and a carrier concentration of $n = 10^{20}$ cm⁻³, the phonon drag still exists in Si and contributes 11% of the total Seebeck coefficient, which translates into 21% of the figure of merit, zT , as zT includes a square term of the Seebeck coefficient. We discuss the mechanisms behind this contribution later in Section II C.

B. Calculated all thermoelectric properties of Si-Ge alloys

We extend the methodology to Si-Ge by adopting a virtual crystal approximation, comparing room-temperature results with experimental data [40,42] in Fig. 1(b), Fig. 2,

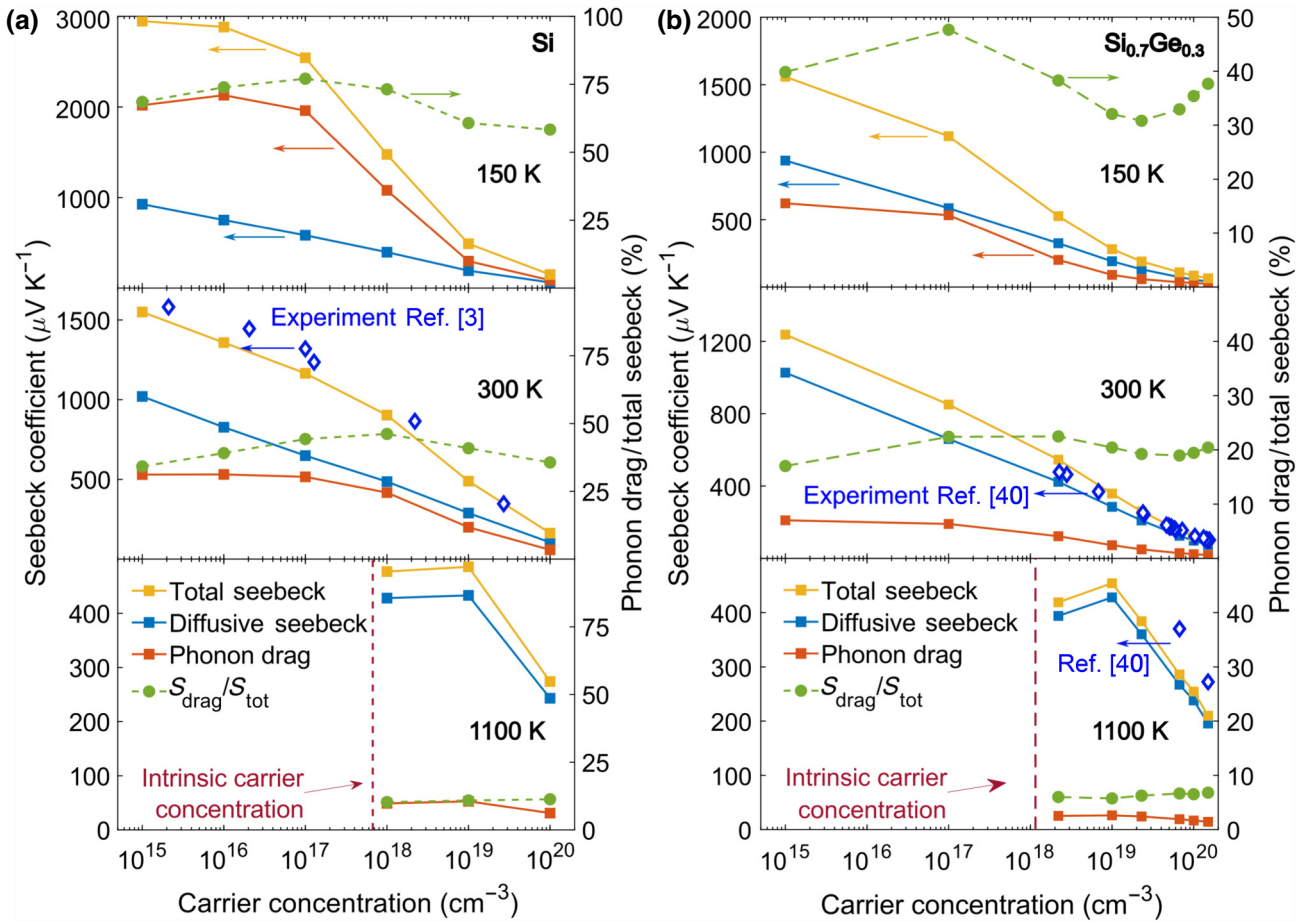


FIG. 1. Phonon drag in Si and $\text{Si}_{0.7}\text{Ge}_{0.3}$. Absolute Seebeck coefficient (left y axis) and relative contribution of phonon drag, S_{drag} , to the total Seebeck coefficient, S_{tot} (right y axis), for n -type Si (a) and $\text{Si}_{0.7}\text{Ge}_{0.3}$ (b) as a function of carrier concentration at 150, 300, and 1100 K. Experimental results (blue diamonds) are from Refs. [3,40].

and Fig. S1 within the Supplemental Material [41], and showing Si-Ge alloys' all thermoelectric properties at 1100 K in Fig. 3. While phonon drag drops with stronger electron-phonon interactions in Fig. 1(b), the decrease in the diffusive Seebeck coefficient is more significant than that in phonon drag as the carrier concentration approaches 10^{20} cm^{-3} , which also results in the increasing relative contribution of phonon drag with higher carrier concentration. Figure 2(a) demonstrates that, at 300 K, it is still essential to include phonon drag in the calculation for heavily doped n -type Si-Ge alloys. Otherwise, the figure of merit, zT , would be underestimated by half. Even at 1100 K and in the heavily doped region ($n \sim 10^{20} \text{ cm}^{-3}$), phonon drag is not trivial, and it still contributes to 10%–20% of zT in Si-Ge alloys [see Fig. 3(a)]. The calculated electrical properties in Figs. 2(a) and 3(b) include electron scattering by equilibrium phonons, the long-range effect of ionized impurity, and the alloying effect. Phonon calculations in Figs. 2(c) and 3(c) take intrinsic three-phonon scattering, phonon scattering by equilibrium electrons, mass disorder, and the boundary into account. While alloying would affect

thermal transport by mass difference and strain fluctuations created by size differences of the atoms, using Klemens' impurity model [43], Abeles found that in Si-Ge alloys the strain contribution to disorder was only about 10% of the mass difference, and the large thermal resistivity was predominantly due to mass-disorder scattering [66]. Thus, we do not include strain scattering in our calculations [more simulation details are given in Supplemental Material Notes [41]] and our calculated total thermal conductivity at 300 K [see Fig. 2(c) and Fig. S1(c) within the Supplemental Material [41]] shows good agreement with experimental data [40,42]. Detailed methods and a discussion of the thermal-conductivity calculations can be found in our previous work [67]. Electron-phonon coupling strength not only affects the mean free paths of phonons and electrons, but also determines how effectively that momentum can be transferred between phonons and electrons. Hence, the magnitude of phonon drag is proportional to the electron-phonon coupling strength, which is reflected in the electron-phonon coupling matrix, $|\langle \mathbf{k}'\beta | \partial_{\mathbf{q}\lambda} V | \mathbf{k}\alpha \rangle|^2$, in the formula for our phonon-drag

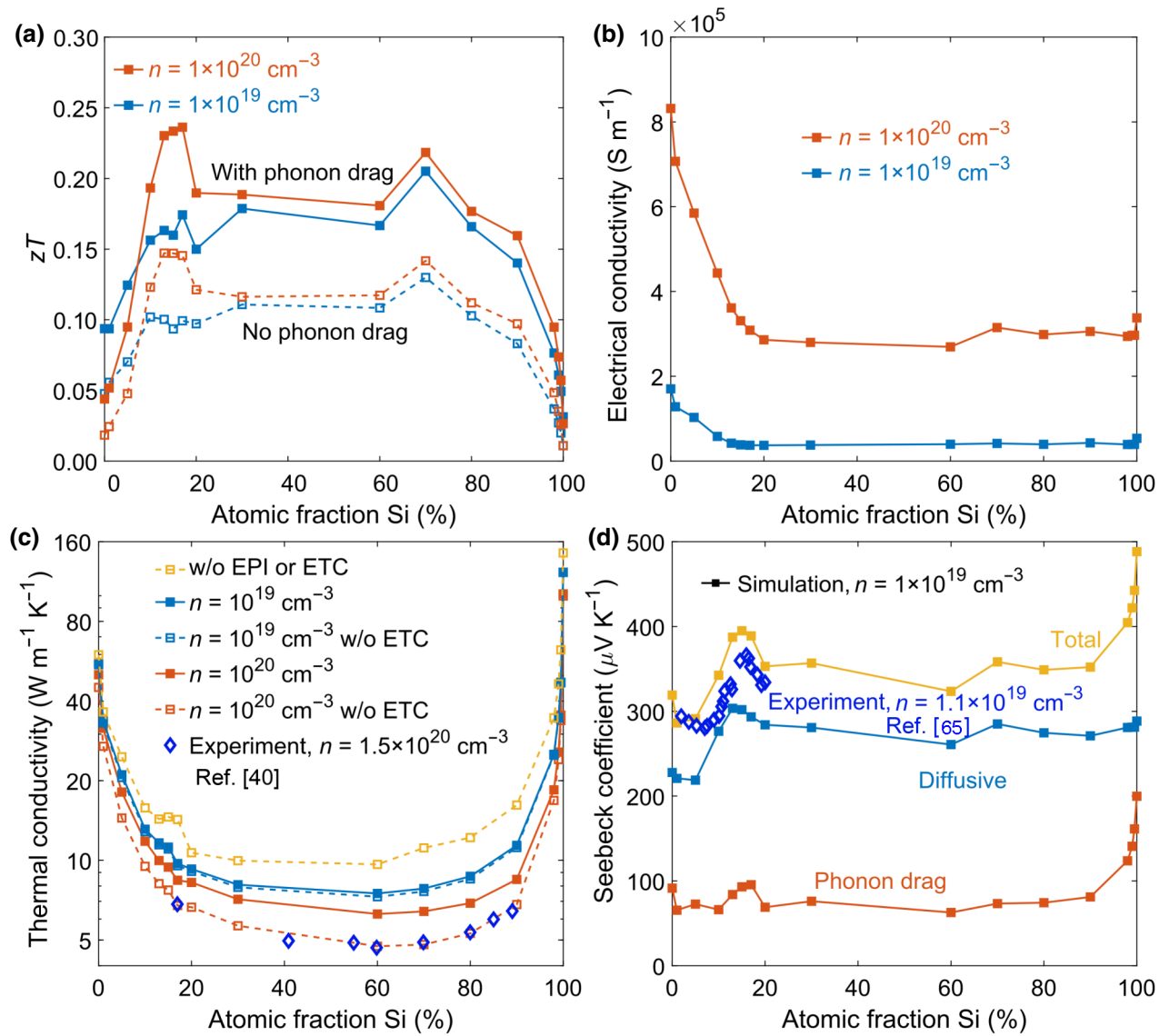


FIG. 2. Thermoelectric properties of n -type Si-Ge alloys at 300 K. (a) Calculated figure of merit, zT , with (solid lines) and without (dashed lines) phonon drag, (b) electrical conductivity, and (c) thermal conductivity at carrier concentrations of $n = 10^{19}$ and 10^{20} cm^{-3} at 300 K. Yellow curve is the lattice thermal conductivity determined by intrinsic three-phonon scattering only, not counting electron-phonon interactions (EPIs) nor electronic thermal conductivity (ETC). Other two dashed lines are lattice thermal conductivity after considering EPIs, while solid lines also include ETC. Experimental data [40] are total thermal conductivity at a carrier concentration of $n = 1.5 \times 10^{20} \text{ cm}^{-3}$. (d) Calculated diffusive part of the Seebeck coefficient (blue), phonon drag (red), and the total Seebeck coefficient (yellow) of n -type Si-Ge at a carrier concentration of $n = 10^{19} \text{ cm}^{-3}$ at 300 K compared with experimental data [65]. Samples in experiment have a carrier concentration of $n = 1.1 \times 10^{19} \text{ cm}^{-3}$, and measurements are performed at 295 K.

calculation [see Eq. (1) in Supplemental Material Note S1 [41]]. We notice that Si has a larger phonon drag than that of Ge. We compare the electron velocities of Si and Ge [see Fig. S14(a) within the Supplemental Material [41]] at their conduction-band edges and find that they are not very different. However, the electron-phonon interaction in Si is stronger, resulting in lower electrical conductivity [shorter electron mean free path in Fig. S14(b) within the Supplemental Material [41]] and larger phonon drag in Figs. 2 and 3. We also study the phonon-scattering rate due

to mass disorder [see Fig. S15(a) within the Supplemental Material [41]] and find that the increase in mass-disorder scattering rate is more significant while alloying Si with Ge in the Si-rich region than that in the Ge-rich region. Accordingly, in a cumulative phonon-drag figure [see Fig. S15(b) within the Supplemental Material [41]], phonons of higher frequency (up to 3 THz) have important contributions to phonon drag in Si, while phonon drag in Ge and the alloys is mostly contributed to by phonons of frequency lower than 1 THz. Therefore, we attribute

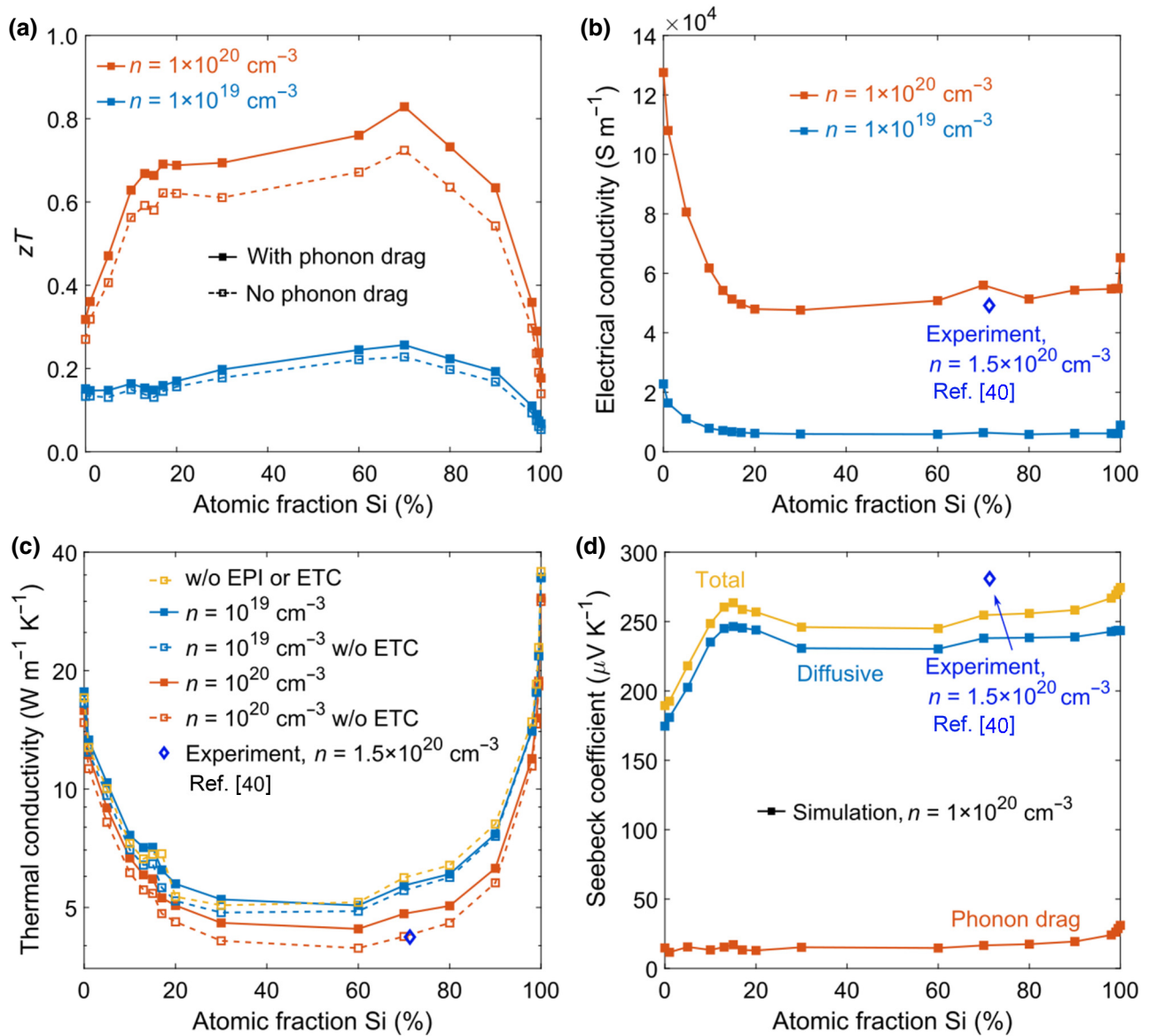


FIG. 3. Thermoelectric properties of n -type Si-Ge alloys at 1100 K. (a) Calculated figure of merit, zT , with (solid lines) and without (dashed lines) phonon drag, (b) electrical conductivity, and (c) thermal conductivity at 1100 K. Yellow curve is lattice thermal conductivity determined by intrinsic three-phonon scattering only, not counting EPIs nor ETC. Other two dashed lines are lattice thermal conductivity after considering EPIs; solid lines also include ETC. Experiments [40] measure total thermal conductivity. (d) Calculated diffusive part of the Seebeck coefficient (blue), phonon drag (red), and the total Seebeck coefficient (yellow) at a carrier concentration of $n = 10^{20} \text{ cm}^{-3}$. Experimental data [40] have a carrier concentration of $n = 1.5 \times 10^{20} \text{ cm}^{-3}$, and measurements are performed at around (b) 1064 K, (c) 1144 K, and (d) 1066 K.

the rapid change in phonon drag with composition in the Si-rich region to changes in both mass-disorder scattering and electron-phonon coupling strength. As shown in Figs. 2(a) and 2(d), the peak in zT in n -type Si-Ge around the composition of $\text{Si}_{0.13}\text{Ge}_{0.87}$ is mainly contributed to by the corresponding peak in the Seebeck coefficient. This is due to band convergence, which results in an increased density of states [38,39] [detailed band structure is given in Fig. S6 within the Supplemental Material [41]], which agrees well with experimental data from Amith's work

[65]. Interestingly, at the band-convergence composition, although a peak exists in the diffusive Seebeck coefficient, the peak in zT is actually largely contributed to by the stronger peak in the phonon-drag part, and this peak in zT becomes less appreciable as phonon drag diminishes with increasing temperature [see Figs. 3(a) and 3(d)]. Although the Seebeck coefficient increases because of the large density of states at band convergence, electron scattering also increases, leading to reduced electron mobility. Another peak in zT around $\text{Si}_{0.7}\text{Ge}_{0.3}$ [see Fig. 3(a) and Figs. S1(a)

and S2(a) within the Supplemental Material [41]) is due to both the low phonon thermal conductivity and electronic contributions. Overall, when the atomic Si percentage is larger than 30% and smaller than 80%, the Si-Ge alloys have comparable electronic properties.

We plot cumulative contributions of different phonon mean free paths to both the phonon-drag Seebeck coefficient [see Fig. 4(a)] and the lattice thermal conductivity [see Fig. 4(b)] in absolute scale for Si, Ge, and $\text{Si}_{0.6}\text{Ge}_{0.4}$ at 1100 K [see Fig. S4 within the Supplemental Material for plots at 150 and 300 K [41]]. Indeed, phonons contributing to phonon drag have a longer mean free path (see Fig. 4) and lower frequency [see Fig. S5 within the Supplemental Material [41]] than those contributing to the lattice thermal conductivity. For instance, in Si and Ge, at $n=10^{20} \text{ cm}^{-3}$ and $T=1100 \text{ K}$ [see Fig. 4 and Fig. S4(b) within the Supplemental Material [41)], phonon drag is contributed to mostly by phonons with a mean free path longer than $0.2 \mu\text{m}$, while approximately 80% of heat conduction is from phonons with a mean free path shorter than $0.2 \mu\text{m}$. The alloy significantly scatters high-frequency phonons with short-to-medium mean free paths, so that the lattice thermal conductivity drops drastically [Fig. 4(b)], leaving longer-mean-free-path phonons contributing more to heat conduction. The alloy does scatter long-mean-free-path phonons to some extent, leading to reduced phonon drag. However, the degrees of the alloy's influence on phonon drag and the lattice thermal conductivity are different, and the alloy serves as a filter that effectively lowers the lattice thermal conductivity without decreasing the Seebeck coefficient significantly.

On the other hand, electron-phonon interactions scatter phonons with a long mean free path, so this reduces phonon drag more than it reduces the thermal conductivity [the difference between the solid lines and dashed lines in Fig. 4(a) is larger than that in Fig. 4(b)]. When the carrier concentration is high, long-mean-free-path phonons are scattered heavily by carriers and phonon drag decreases considerably. At 1100 K, when the carrier concentration increases from $n=10^{19} \text{ cm}^{-3}$ (Fig. 4, solid lines) to $n=10^{20} \text{ cm}^{-3}$ (Fig. 4, dashed lines), phonon-drag values of Si, Ge, and $\text{Si}_{0.6}\text{Ge}_{0.4}$ decrease by 70%, 37%, and 46%, respectively, but thermal-conductivity values drop only by 15%, 12%, and 24%, respectively. The latter matches our previous conclusion [67] that the reduction in lattice thermal conductivity due to electron-phonon interactions in alloys is more significant than that in Si and Ge: the mass difference in Si-Ge alloys screens out the high-frequency phonons with short-to-medium mean free paths and leaves the long-mean-free-path phonons subject to scattering by electrons contributing more to the lattice thermal conductivity. Nevertheless, for phonon drag, we cannot draw the same conclusion because, in addition to the alloying effect, the electron-phonon coupling strength, which is a

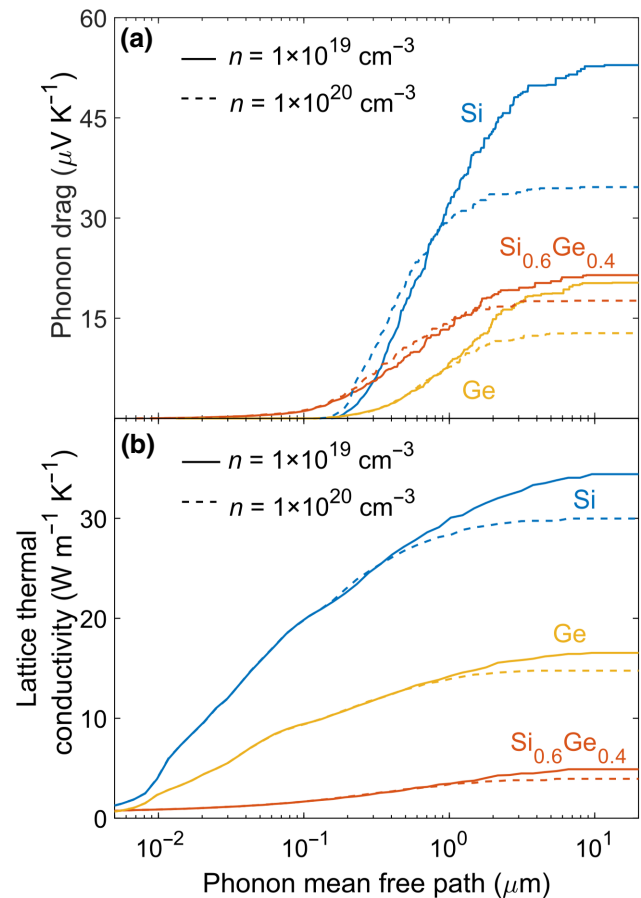


FIG. 4. Absolute cumulative contributions of phonons with different mean free paths to phonon drag and lattice thermal conductivity at 1100 K. Calculated cumulative (a) phonon drag and (b) lattice thermal conductivity for n -type Si (blue), Ge (yellow), and $\text{Si}_{0.6}\text{Ge}_{0.4}$ (red) at 1100 K at two different carrier concentrations: 10^{19} cm^{-3} (solid lines) and 10^{20} cm^{-3} (dashed lines). Comparison between solid and dashed lines demonstrates the effect of electron-phonon interactions: electron-phonon interactions have larger impacts on phonon drag than on lattice thermal conductivity.

deciding factor of phonon drag, also depends on the alloy's composition.

When the temperature increases, the two features discussed above, regarding the alloying effect and electron-phonon interactions, still hold true. But the entire accumulation spectrum would shift to a shorter mean free path, as a result of the change in phonon population and intrinsic phonon-phonon scattering strength.

We further present the thermoelectric properties of $\text{Si}_{0.7}\text{Ge}_{0.3}$ from 150 to 1100 K (see Fig. 5) to demonstrate our method's predictive power, since the thermoelectric properties of $\text{Si}_{0.7}\text{Ge}_{0.3}$ across a wide range of temperatures are available from experimental work by Dismukes *et al.* [40]. The overall trend of our results agrees with experiments. The discrepancy between our calculated figure of

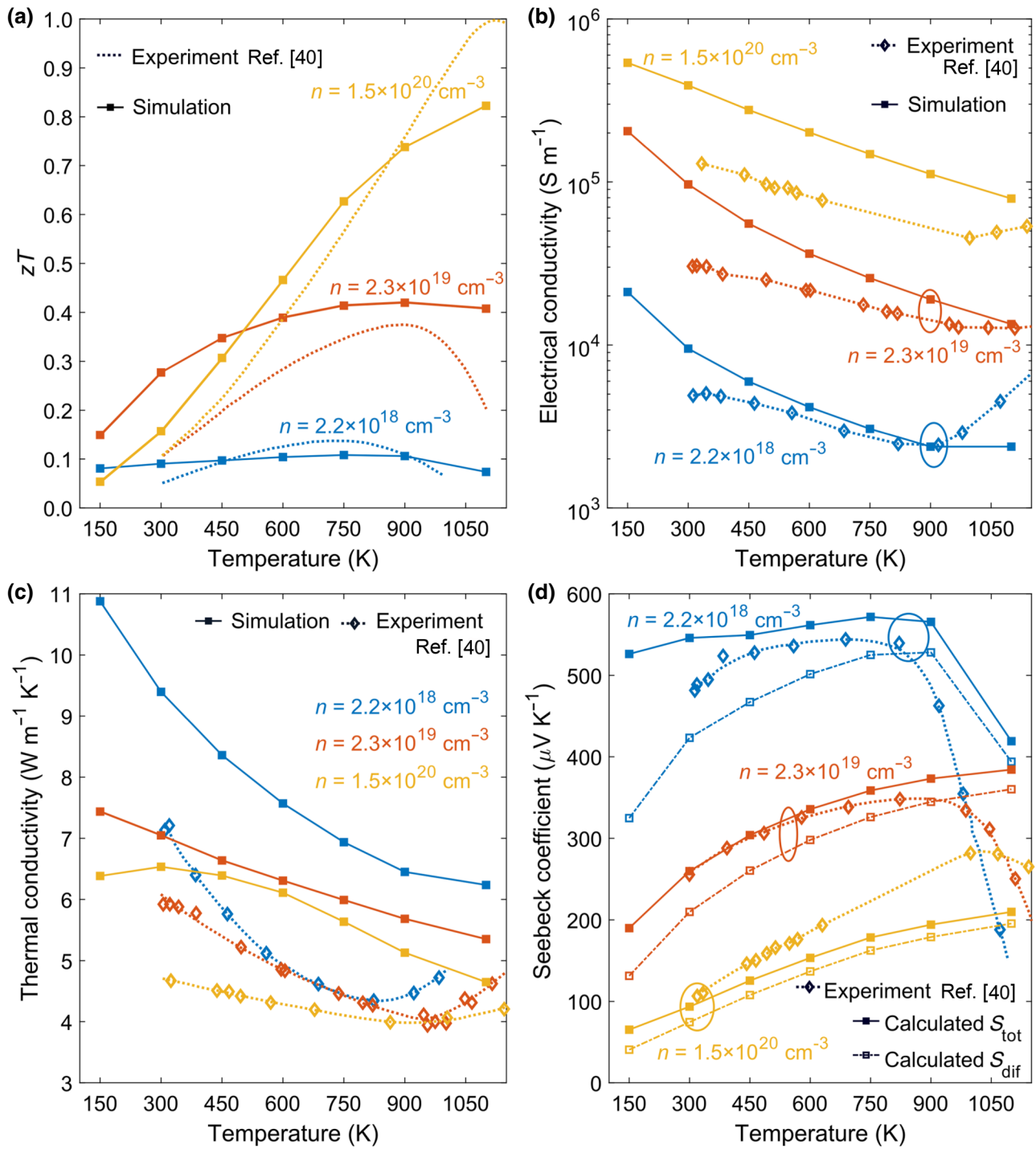


FIG. 5. Comparison of calculated and experimental thermoelectric properties of n -type $\text{Si}_{0.7}\text{Ge}_{0.3}$ as a function of temperature at three different carrier concentrations. (a) Figure of merit, zT ; (b) electrical conductivity; (c) thermal conductivity, including electronic thermal conductivity; and (d) Seebeck coefficient (both diffusive S_{dif} and total S_{tot} are shown). At 1100 K and $n = 1.5 \times 10^{20} \text{ cm}^{-3}$, phonon drag contributes to about 7% of the Seebeck coefficient and about 13% of zT . Experimental data are from Ref. [40].

merit, zT , and the experimental data could arise for the following reasons. (1) The band structure generated by DFT may not be entirely accurate, especially for Ge-rich alloys. Band structures used in transport-property calculations are after Wannier interpolation, which can have small

deviations from as-calculated results of electronic band calculations [Fig. S6(b) within the Supplemental Material [41]]. In heavily doped materials, a strong coupling between dopants and the host material can alter the band structure. We do not have this feature in our current

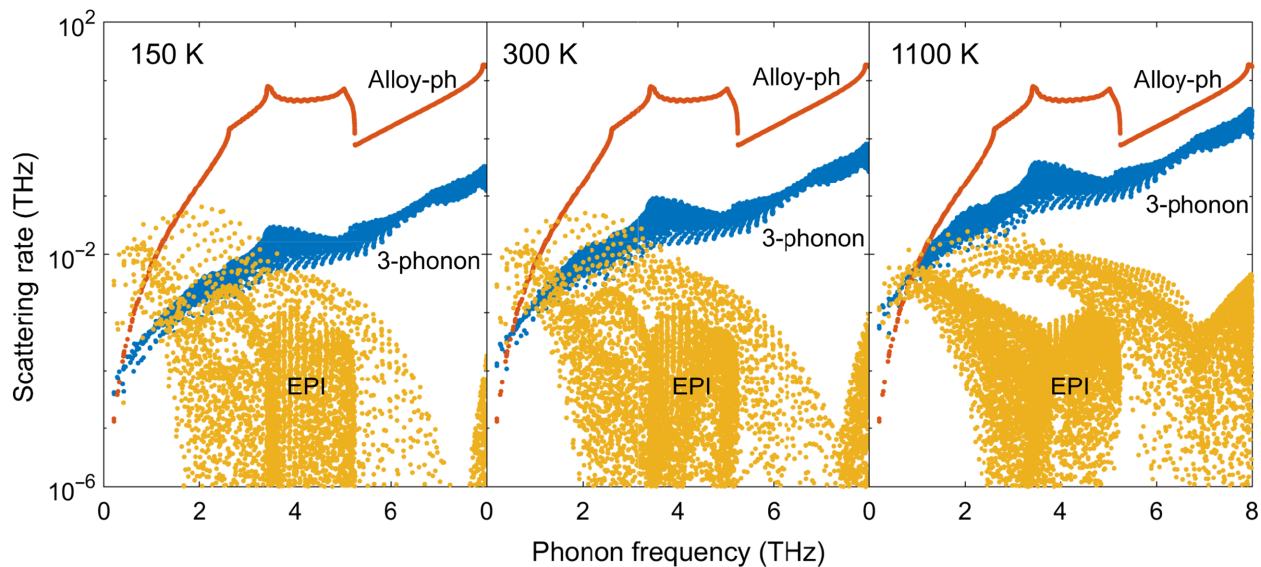


FIG. 6. Comparison of phonon-scattering rates in heavily doped n -type $\text{Si}_{0.7}\text{Ge}_{0.3}$ at different temperatures. Phonon-scattering rates of intrinsic three-phonon scattering (“3-phonon,” blue), alloy mass-disorder scattering (“alloy-ph,” red), and EPI (yellow) at 150 K (left), 300 K (middle), and 1100 K (right). Carrier concentration is kept at $n = 10^{20} \text{ cm}^{-3}$ at all three temperatures.

simulations. An inaccuracy in the band shape would cause an error in the electrical conductivity, and an inaccuracy in the band gap could affect the bipolar effects in the electrical conductivity, the thermal conductivity, and the Seebeck coefficient. (2) We use the Brooks-Herring model in our ionized-impurity scattering calculation, which assigns electrons to plane-wave states and does not consider the core scattering of ionized impurities. Figure S11 within the Supplemental Material [41] gives a comparison of calculated and measured electron mobilities in Si, $\text{Si}_{0.2}\text{Ge}_{0.8}$, and Ge at different carrier concentrations. The electrical conductivity calculations can be further improved by incorporating short-range core scattering by dopants. (3) In experiments, the sample carrier concentrations are measured at high temperatures and can change with temperature due to the thermal activation of dopants [40]. In our simulations, materials have fixed net carrier concentrations at all temperatures. Hence, the “rising tails” in experimental data in Figs. 5(b) and 5(c), resulting from bipolar electrical conductivity and bipolar thermal conductivity, are not well captured. (4) We include only the three-phonon process as the intrinsic phonon-phonon scattering in our calculation of the lattice thermal conductivity, while the four-phonon process can be important at high temperatures [68,69]. Given that the strength of four-phonon scattering scales quadratically with temperature [69], we estimate that the lattice thermal conductivity of Si-Ge alloys at 1100 K determined only by the three-phonon process would be about 25% higher than that considering both three-phonon and four-phonon processes. (5) The virtual crystal approximation is only a first-order

approximation. It models alloy systems as homogeneous crystals and cannot capture many other disordered features in real alloy materials (especially in heavily doped samples), e.g., dislocations, stacking faults, vacancies or vacancy complexes, and other defects. (6) The current approach relies on several approximations that neglect higher-order effects: phonon scattering by equilibrium electrons, electron scattering by equilibrium phonons, the relaxation approximation, and the after-scattering state described as the undisturbed Bloch state of the periodic host lattice within the first Born approximation. (7) According to our convergence test [see Figs. S9 and S10 within the Supplemental Material [41]], we estimate that there might be up to 10% error in our current results, compared with the ideally converged results if denser meshes were allowed by computing power.

C. Competition of phonon scattering mechanisms

Our results show that, even at 1100 K and in the heavily doped region ($n \sim 10^{20} \text{ cm}^{-3}$), phonon drag is not trivial in Si-Ge alloys, and it still contributes to 10%–20% of zT [see Fig. 3(a) and Fig. S2(a) within the Supplemental Material [41]]. As shown in Fig. 1, surprisingly, phonon drag’s relative contribution can increase with carrier concentration at 1100 K. From the spectral analysis of phonons, we attribute this nonintuitive phenomenon to competition between several phonon-scattering mechanisms. We already know that low-frequency phonons are those participating in phonon drag [see Fig. S5 within the Supplemental Material [41]], thus the dominant

scattering of these phonons determines their mean free path and largely determines phonon drag. Taking $\text{Si}_{0.7}\text{Ge}_{0.3}$ as an example, we compare the three phonon-scattering rates (intrinsic three-phonon scattering, phonon scattering by mass disorder, and phonon scattering by electrons) in Fig. 6. At lower temperatures, phonon drag is more sensitive to carrier concentration, since the intrinsic phonon scattering is weak, so it is easier for phonon scattering by electrons to surpass the intrinsic phonon scattering and become the dominant scattering mechanism for phonons contributing to phonon drag. At 1100 K, the intrinsic phonon scattering is so strong that electron-phonon scattering barely affects the low-frequency phonons' mean free path, unless the carrier concentration becomes extremely high ($n > 10^{20} \text{ cm}^{-3}$). In such a case, before entering the extremely heavily doped region, phonon drag stays almost constant, while the diffusive part of the Seebeck coefficient decreases with increasing carrier concentration, so the relative contribution of phonon drag to the total Seebeck coefficient can become more appreciable in the heavily doped Si-Ge alloy. On the other hand, in $\text{Si}_{0.7}\text{Ge}_{0.3}$, the decrease in the diffusive Seebeck coefficient with stronger electron-phonon interactions is more significant than that in phonon drag in Fig. 1(b) at 150 and 300 K as the carrier concentration approaches 10^{20} cm^{-3} , but the increasing relative contribution of phonon drag with higher carrier concentration in $\text{Si}_{0.7}\text{Ge}_{0.3}$ is not observed in Si at 150 and 300 K. This is because electron-phonon interactions have a smaller impact on phonon drag in the $\text{Si}_{0.7}\text{Ge}_{0.3}$ alloy than that in Si (due to stronger scattering of long-mean-free-path phonons by mass disorder in $\text{Si}_{0.7}\text{Ge}_{0.3}$, weaker intrinsic phonon scattering, and stronger electron-phonon interactions in Si) at these temperatures, as shown by the cumulative contributions of electrons with different mean free paths to the diffusive Seebeck coefficient and phonon drag at $n = 10^{19}$ and 10^{20} cm^{-3} in Si and $\text{Si}_{0.7}\text{Ge}_{0.3}$, [see Fig. S16 within the Supplemental Material [41]].

III. CONCLUSION

We calculate the Seebeck coefficient, the electrical conductivity, and the thermal conductivity, and obtain zT of both n -type and p -type Si-Ge alloys [data for p -type material are available in the Supplemental Material [41]] over the complete range of compositions at different carrier concentrations (10^{15} to 10^{20} cm^{-3}) from 150 to 1100 K. In particular, we include the phonon-drag part of the contribution in our Seebeck calculations and take both alloy scattering of phonons and alloy scattering of electrons into account. Contrary to conventional wisdom that phonon drag would disappear in alloy-based thermoelectric materials [9] or at high temperatures, we find that phonon drag contributes significantly to the total Seebeck coefficient in Si-Ge alloys: even at 1100 K, phonon drag still contributes to 10%–20% of zT and its relative contribution

to the total Seebeck coefficient can increase with higher carrier concentration. Our first-principles calculation successfully reproduces the peak in the measured Seebeck coefficient around the composition of n -type $\text{Si}_{0.13}\text{Ge}_{0.87}$ due to band convergence and highlights the competition between band convergence increasing the Seebeck coefficient with increased scattering and lower mobility. This work demonstrates that all thermoelectric transport properties of alloy-based practical thermoelectric materials can be simulated from first principles. The insights gained here are essential for understanding thermoelectric transport and improving the performance of state-of-the-art thermoelectric materials.

IV. METHODS

A. DFT calculations

The $\text{Si}_x\text{Ge}_{1-x}$ alloy crystal is generated by compositionally averaging the masses and pseudopotentials of Si and Ge (Si.pz-n-nc.UPF and Ge.pz-n-nc.UPF), and the linearly interpolated lattice constants are used as initial inputs to get the final relaxed structure. The electronic Hamiltonian, dynamical matrix, and phonon perturbation are obtained from density-functional-theory calculations using the QUANTUM ESPRESSO software [44]. The kinetic energy cutoff for wave functions is 80 Rydberg; the convergence threshold for self-consistency is 10^{-12} Rydberg. Electronic band calculations use a $12 \times 12 \times 12$ Monkhorst-Pack [70] k -mesh phonon band and perturbation calculations use a $6 \times 6 \times 6$ Monkhorst-Pack q mesh. Electronic Wannier functions and phonon perturbation in the Wannier representation constructed from information obtained on the coarse meshes outlined above are interpolated to an $80 \times 80 \times 80$ k mesh and an $80 \times 80 \times 80$ q mesh to calculate the electron-phonon matrix element using the EPW code [45–47]. We do the same interpolation for the alloy-electron scattering-rate calculations in parallel by substituting the electron-phonon interaction matrix with the alloy-electron interaction matrix using the perturbed potential obtained in alloy-electron scattering. The lattice thermal-conductivity calculations within the relaxation-time approximation to the phonon Boltzmann transport equation are carried out with our modified ShengBTE package [48] using a $60 \times 60 \times 60$ q mesh. More details on thermal-conductivity calculations can be found in our previous work [67]. Methods of calculating phonon drag and addressing different scattering mechanisms of phonons and electrons are given in the Supplemental Material [41].

Data that support the plots and other findings of this study are available from the lead contact on reasonable request. The code for computing electron-phonon scattering rates through first-principles calculation is a modified version of the EPW [45,46] code, released initially within the QUANTUM ESPRESSO [44] package. Our modified EPW code is available, see Ref. [47].

ACKNOWLEDGMENTS

We thank Professor Evelyn Wang for her helpful comments. This work is partially supported by the Defense Advanced Research Projects Agency (DARPA) Materials for Transduction (MATRIX) program, under Grant No. HR0011-16-2-0041 (for developing and applying the simulation codes to assist MATRIX teams, August 2016 to August 2019).

Q.X., J.Z., and T.L. contributed to coding. Q.X. performed the first-principles calculations, analyzed data, and wrote the manuscript. G.C. supervised the research. All authors commented on, discussed, and edited the manuscript.

The authors declare no conflict of interest.

-
- [1] T. H. Geballe and G. W. Hull, Seebeck effect in germanium, *Phys. Rev.* **94**, 1134 (1954).
- [2] C. Herring, Theory of the thermoelectric power of semiconductors, *Phys. Rev.* **96**, 1163 (1954).
- [3] T. H. Geballe and G. W. Hull, Seebeck effect in silicon, *Phys. Rev.* **98**, 940 (1955).
- [4] I. Weinberg, Phonon-drag thermopower in Cu-Al and Cu-Si alloys, *Phys. Rev.* **729**, 838 (1965).
- [5] A. R. Hutson, Electronic properties of ZnO, *J. Phys. Chem. Solids* **8**, 467 (1959).
- [6] C. C. Lee and P. A. Schroeder, Phonon drag thermopower in silver alloys, *Philos. Mag.* **25**, 1161 (1972).
- [7] A. Bentien, S. Johnsen, G. K. H. Madsen, B. B. Iversen, and F. Steglich, Colossal seebeck coefficient in strongly correlated semiconductor FeSb₂, *Europhys. Lett.* **80**, 17008 (2007).
- [8] H. Takahashi, R. Okazaki, S. Ishiwata, H. Taniguchi, A. Okutani, M. Hagiwara, and I. Terasaki, Colossal seebeck effect enhanced by quasi-ballistic phonons dragging massive electrons in FeSb₂, *Nat. Commun.* **7**, 1 (2016).
- [9] G. A. Slack and M. A. Hussain, The maximum possible conversion efficiency of silicon-germanium thermoelectric generators, *J. Appl. Phys.* **70**, 2694 (1991).
- [10] *CRC Handbook of Thermoelectrics*, *CRC Handbook of Thermoelectrics*, edited by D. Rowe (CRC Press, Boca Raton, Florida, 1995).
- [11] J. Sadhu, H. Tian, J. Ma, B. Azeredo, J. Kim, K. Balasundaram, C. Zhang, X. Li, P. M. Ferreira, and S. Sinha, Quenched phonon drag in silicon nanowires reveals significant effect in the bulk at room temperature, *Nano Lett.* **15**, 3159 (2015).
- [12] A. I. Boukai, Y. Bunimovich, J. Tahir-Kheli, J. K. Yu, W. A. Goddard, and J. R. Heath, Silicon nanowires as efficient thermoelectric materials, *Nature* **451**, 168 (2008).
- [13] A. S. Yalamarthy, M. Muñoz Rojo, A. Bruefach, D. Boone, K. M. Dowling, P. F. Satterthwaite, D. Goldhaber-Gordon, E. Pop, and D. G. Senesky, Significant phonon drag enables high power factor in the AlGa_N/Ga_N two-dimensional electron gas, *Nano Lett.* **19**, 3770 (2019).
- [14] J. M. Ziman and P. W. Levy, Electrons and phonons, *Phys. Today* **14**, 64 (1961).
- [15] H. P. R. Frederikse, Thermoelectric power of germanium below room temperature, *Phys. Rev.* **92**, 248 (1953).
- [16] M. Bailyn, Transport in metals: Effect of the nonequilibrium phonons, *Phys. Rev.* **112**, 1587 (1958).
- [17] M. E. Brinson and W. Dunstant, Thermal conductivity and thermoelectric power of heavily doped n-type silicon, *J. Phys. C: Solid State Phys.* **3**, 483 (1970).
- [18] E. Behnen, Quantitative examination of the thermoelectric power of n-type Si in the phonon drag regime, *J. Appl. Phys.* **67**, 287 (1990).
- [19] G. D. Mahan, L. Lindsay, and D. A. Broido, The Seebeck coefficient and phonon drag in silicon, *J. Appl. Phys.* **116**, 245102 (2014).
- [20] N. H. Protik and D. A. Broido, Coupled transport of phonons and carriers in semiconductors: A case study of n-doped GaAs, *Phys. Rev. B* **101**, 075202 (2020).
- [21] J. Zhou, B. Liao, B. Qiu, S. Huberman, K. Esfarjani, M. S. Dresselhaus, and G. Chen, Ab initio optimization of phonon drag effect for lower-temperature thermoelectric energy conversion, *Proc. Natl. Acad. Sci. U. S. A.* **112**, 14777 (2015).
- [22] M. Fiorentini and N. Bonini, Thermoelectric coefficients of n-doped silicon from first principles via the solution of the Boltzmann transport equation, *Phys. Rev. B* **94**, 085204 (2016).
- [23] R. Trzcinski, E. Gmelin, and H. J. Queisser, Quenched Phonon Drag in Silicon Microcontacts, *Phys. Rev. Lett.* **56**, 1086 (1986).
- [24] P. G. Klemens, in *Fifteenth International Conference on Thermoelectrics. Proceedings ICT'96* (1996), pp. 206–208.
- [25] D. M. Rowe, V. S. Shukla, and N. Savvides, Phonon scattering at grain boundaries in heavily doped fine-grained silicon-germanium alloys, *Nature* **290**, 765 (1981).
- [26] X. W. Wang, H. Lee, Y. C. Lan, G. H. Zhu, G. Joshi, D. Z. Wang, J. Yang, A. J. Muto, M. Y. Tang, J. Klatsky, S. Song, M. S. Dresselhaus, G. Chen, and Z. F. Ren, Enhanced thermoelectric figure of merit in nanostructured n-type silicon germanium bulk alloy, *Appl. Phys. Lett.* **93**, 1 (2008).
- [27] G. Joshi, H. Lee, Y. Lan, X. Wang, G. Zhu, D. Wang, R. W. Gould, D. C. Cuff, M. Y. Tang, M. S. Dresselhaus, *et al.*, Enhanced thermoelectric figure-of-merit in nanostructured p-type silicon germanium bulk alloys, *Nano Lett.* **8**, 4670 (2008).
- [28] J. Garg, N. Bonini, B. Kozinsky, and N. Marzari, Role of Disorder and Anharmonicity in the Thermal Conductivity of Silicon-Germanium Alloys: A First-Principles Study, *Phys. Rev. Lett.* **106**, 45901 (2011).
- [29] G. J. Snyder and E. S. Toberer, Complex thermoelectric materials, *Nat. Mater.* **7**, 105 (2008).
- [30] S. K. Bux, R. G. Blair, P. K. Gogna, H. Lee, G. Chen, M. S. Dresselhaus, R. B. Kaner, and J. P. Fleurial, Nanostructured bulk silicon as an effective thermoelectric material, *Adv. Funct. Mater.* **19**, 2445 (2009).
- [31] P. H. Jiang, H. J. Liu, L. Cheng, D. D. Fan, J. Zhang, J. Wei, J. H. Liang, and J. Shi, Thermoelectric properties of γ -graphyne from first-principles calculations, *Carbon N. Y.* **113**, 108 (2017).
- [32] T. Ouyang, E. Jiang, C. Tang, J. Li, C. He, and J. Zhong, Thermal and thermoelectric properties of

- monolayer indium triphosphide (InP₃): A first-principles study, *J. Mater. Chem. A* **6**, 21532 (2018).
- [33] X. L. Zhu, P. F. Liu, J. Zhang, P. Zhang, W. X. Zhou, G. Xie, and B. T. Wang, Monolayer SnP₃: An excellent p-type thermoelectric material, *Nanoscale* **11**, 19923 (2019).
- [34] R. Guo, X. Wang, Y. Kuang, and B. Huang, First-Principles study of anisotropic thermoelectric transport properties of IV-VI semiconductor compounds SnSe and SnS, *Phys. Rev. B: Condens. Matter Mater. Phys.* **92**, 115202 (2015).
- [35] E. Haque and M. A. Hossain, First-Principles study of elastic, electronic, thermodynamic, and thermoelectric transport properties of TaCoSn, *Results Phys.* **10**, 458 (2018).
- [36] T. H. Liu, J. Zhou, M. Li, Z. Ding, Q. Song, B. Liao, L. Fu, and G. Chen, Electron mean-free-path filtering in dirac material for improved thermoelectric performance, *Proc. Natl. Acad. Sci. U. S. A.* **115**, 879 (2018).
- [37] S. Duan, Y. Cui, X. Chen, W. Yi, Y. Liu, and X. Liu, Ultra-high thermoelectric performance realized in black phosphorus system by favorable band engineering through group VA doping, *Adv. Funct. Mater.* **29**, 1904346 (2019).
- [38] Y. Pei, X. Shi, A. Lalonde, H. Wang, L. Chen, and G. J. Snyder, Convergence of electronic bands for high performance bulk thermoelectrics, *Nature* **473**, 66 (2011).
- [39] Y. Pei, H. Wang, and G. J. Snyder, Band engineering of thermoelectric materials, *Adv. Mater.* **24**, 6125 (2012).
- [40] J. P. Dismukes, L. Ekstrom, E. F. Steigmeier, I. Kudman, and D. S. Beers, Thermal and electrical properties of heavily doped Ge-Si alloys up to 1300 K, *J. Appl. Phys.* **35**, 2899 (1964).
- [41] See the Supplemental Material at <http://link.aps.org/supplemental/10.1103/PhysRevApplied.16.064052>, for Refs. [21, 28,40,42–63], more simulation results, details of the phonon-drag calculation, and scattering mechanisms of phonons and electrons, as referenced throughout the text.
- [42] M. C. Steele and F. D. Rosi, Thermal conductivity and thermoelectric power of germanium-silicon alloys, *J. Appl. Phys.* **29**, 1517 (1958).
- [43] P. G. Klemens, The scattering of low-frequency lattice waves by static imperfections, *Proc. Phys. Soc. Sect. A* **68**, 1113 (1955).
- [44] P. Giannozzi, *et al.*, QUANTUM ESPRESSO: A modular and open-source software project for quantum simulations of materials, *J. Phys. Condens. Matter* **21**, 395502 (2009).
- [45] F. Giustino, M. L. Cohen, and S. G. Louie, Electron-phonon interaction using wannier functions, *Phys. Rev. B: Condens. Matter Mater. Phys.* **76**, 165108 (2007).
- [46] S. Ponc e, E. R. Margine, C. Verdi, and F. Giustino, EPW: Electron-phonon coupling, transport and superconducting properties using maximally localized wannier functions, *Comput. Phys. Commun.* **209**, 116 (2016).
- [47] J. Zhou, T. Liu, Q. Song, Q. Xu, Z. Ding, B. Liao, and G. Chen, First-principles simulation of electron transport and thermoelectric property of materials, including electron-phonon scattering, defect scattering, and phonon drag, Materials Cloud Archive 2020.106 (2020).
- [48] W. Li, J. Carrete, N. A. Katcho, and N. Mingo, ShengBTE: A solver of the boltzmann transport equation for phonons, *Comput. Phys. Commun.* **185**, 1747 (2014).
- [49] F. Mousty, P. Ostojia, and L. Passari, Relationship between resistivity and phosphorus concentration in silicon, *J. Appl. Phys.* **45**, 4576 (1974).
- [50] J. C. Irvin, Resistivity of bulk silicon and of diffused layers in silicon, *Bell Syst. Tech. J.* **41**, 387 (1962).
- [51] V. I. Fistul, M. I. Iglitsyn, and E. M. Omelyanovskii, Mobility of electrons in germanium strongly doped with arsenic, mobility of electrons in germanium strongly doped with arsenic, *Sov. Phys.-Solid State* **4**, 784 (1962).
- [52] S. Tamura, Isotope scattering of dispersive phonons in Ge, *Phys. Rev. B* **27**, 858 (1983).
- [53] D. G. Cantrell and P. N. Butcher, A calculation of the phonon-drag contribution to the thermopower of quasi-2D electrons coupled to 3D phonons. I. general theory, *J. Phys. C: Solid State Phys.* **20**, 1985 (1987).
- [54] N. W. Ashcroft and N. D. Mermin, *Solid State Physics, Solid State Physics* (Rinehart and Winston, Holt, 1976).
- [55] A. Kundu, N. Mingo, D. A. Broido, and D. A. Stewart, Role of light and heavy embedded nanoparticles on the thermal conductivity of SiGe alloys, *Phys. Rev. B* **84**, 125426 (2011).
- [56] S. Huberman, V. Chiloyan, R. A. Duncan, L. Zeng, R. Jia, A. A. Maznev, E. A. Fitzgerald, K. A. Nelson, and G. Chen, Unifying first-principles theoretical predictions and experimental measurements of size effects in thermal transport in SiGe alloys, *Phys. Rev. Mater.* **1**, 54601 (2017).
- [57] J. Zhou, B. Liao, and G. Chen, First-Principles calculations of thermal, electrical, and thermoelectric transport properties of semiconductors, *Semicond. Sci. Technol.* **31**, 043001 (2016).
- [58] H. B. G. Casimir, Note on the conduction of heat in crystals, *Physica* **5**, 495 (1938).
- [59] H. Brooks, Scattering by ionized impurities in semiconductors, scattering by ionized impurities in semiconductors, *Phys. Rev.* **83**, 879 (1951).
- [60] M. Lundstrom, *Fundamentals of Carrier Transport, Fundamentals of Carrier Transport* (Cambridge University Press, Cambridge, 2009).
- [61] D. Chattopadhyay and H. J. Queisser, Electron scattering by ionized impurities in semiconductors, *Rev. Mod. Phys.* **53**, 745 (1981).
- [62] Felipe Murphy-Armando and S. Fahy, First-Principles Calculation of Alloy Scattering in Ge_xSi_{1-x}, *Phys. Rev. Lett.* **97**, 96606 (2006).
- [63] F. Murphy-Armando and S. Fahy, First-Principles calculation of carrier-phonon scattering in n-type Si_{1-x}Ge_x alloys, *Phys. Rev. B* **78**, 35202 (2008).
- [64] B. Liao, B. Qiu, J. Zhou, S. Huberman, K. Esfarjani, and G. Chen, Significant Reduction of Lattice Thermal Conductivity by the Electron-Phonon Interaction in Silicon With High Carrier Concentrations: A First-Principles Study, *Phys. Rev. Lett.* **114**, 115901 (2015).
- [65] A. Amith, Seebeck coefficient in N-type germanium-silicon alloys: “competition” region, *Phys. Rev.* **139**, 1624 (1965).
- [66] B. Abeles, Lattice thermal conductivity of disordered semiconductor alloys at high temperatures, *Phys. Rev.* **104**, 1906 (1963).
- [67] Q. Xu, J. Zhou, T. H. Liu, and G. Chen, Effect of electron-phonon interaction on lattice thermal

- conductivity of SiGe alloys, *Appl. Phys. Lett.* **115**, 023903 (2019).
- [68] T. Feng, L. Lindsay, and X. Ruan, Four-phonon scattering significantly reduces intrinsic thermal conductivity of solids, *Phys. Rev. B* **96**, 161201 (2017).
- [69] X. Gu and C. Y. Zhao, Thermal conductivity of hexagonal Si, Ge, and $\text{Si}_{1-x}\text{Ge}_x$ alloys from first-principles, *J. Appl. Phys.* **123**, 185104 (2018).
- [70] H. J. Monkhorst and J. D. Pack, Special points for brillouin-zone integrations, *Phys. Rev. B* **13**, 5188 (1976).